Reconfigurable frequency demultiplexer using coupled-resonator elastic waveguides

Yi-Ming Cui,[1,2,a)] Hao-Ran Dong,[1,2,a)] Yan-Feng Wang,[1,2,b)] Vincent Laude,[3] and Yue-Sheng Wang[1,4]
[1)]*School of Mechanical Engineering, Tianjin University, 300350 Tianjin, China*
[2)]*National Key Laboratory of Vehicle Power System, Tianjin 300350, China*
[3)]*Institut FEMTO-ST, CNRS, Université de Franche-Comté, F-25000 Besançon, France*
[4)]*Institute of Engineering Mechanics, Beijing Jiaotong University, Beijing 100044, China*

(*Electronic mail: wangyanfeng@tju.edu.cn)

(Dated: 28 August 2024)

Reconfigurable coupled-resonator elastic waveguides (CREW) are formed using defects composed of threaded rods, fixed with nuts and attached to a perforated two-dimensional phononic crystal slab. The resonant frequency of the defect can be tuned continuously within a complete phononic band gap by adjusting the length of the threaded rod. Straight waveguides are formed from a line of defects. Phononic circuits are created by coupling three parallel straight waveguides. Through precise manipulation of the length of the threaded rod assembly, frequency demultiplexing of Lamb waves is achieved. Numerical and experimental results are found to be in good agreement. This work is of significance for the practical design of phononic devices including reconfigurable circuits.

The study of modulating elastic waves in artificial periodic structures has attracted a lot of attention[1,2]. Phononic crystals (PCs)[3,4], as a functional composite material with spatial periodicity, are characterized by bandgap[5,6]. In the frequency range where the bandgap is located, the propagation of elastic/acoustic waves is forbidden, and only evanescent waves with spatial attenuation are allowed[7], which gives phononic crystals applications in vibration isolation[8], filtering[9], and so on. The introduction of defects breaks the original periodicity and defect states can arise inside bandgaps. As a result, waves can propagate along a linear chain of defect cavities[10]. Novel elastic wave devices can be designed, e.g. waveguides[11], splitters[12], multiplexers and demultiplexers[13,14].

Recently, the propagation of Lamb waves in defect chains[15–17] has been increasingly studied. Based on linear waveguides, the concept of coupled-resonator optical waveguides (CROWs)[18] was first introduced in the field of photonics. Subsequently, the concepts of CREWs[16] and coupled-resonator acoustic waveguides (CRAWs) inspired by CROWs were proposed. The wave amplitude decays exponentially as it moves away from the defect, enabling strong localization and low group velocity transmission[19] of waves in CREWs. Theoretically, CREWs can be designed for arbitrary acoustic lines[20–22]. Wang et al. realized multiple bending waveguides based on CREWs[17,23]. Ji et al. proposed a CRAW model by arranging scatterers made of square shape memory alloy in a water matrix[24]. Escalante et al. investigate the dispersion of CRAW formed by evanescent coupling of a chain of defect cavities[25].

Although PCs exhibit the properties discussed above, they rarely have real-life applications. Most PC-based devices operate in fixed frequency ranges. The material and geometrical parameters are hardly tunable or reconfigurable after fabrication. Since elastic wave propagation is mainly controlled by material properties and geometry parameters, extensive research has been conducted on tunable and reconfigurable manipulation of acoustic and elastic waves. Tunable phononic crystals[1] achieve control over material parameters through physical fields, such as altering the electric field[26], magnetic field[27], thermal field[28], etc. Reconfigurable phononic crystals[29], on the other hand, modify their geometric structure through mechanical means, changing the magnitude of prestress in the structure[30], introducing fluid into predetermined holes[31,32], or other methods to control wave propagation.

In this letter, we demonstrate a novel approach for demultiplexing Lamb waves in the frequency and space domain using reconfigurable CREWs. Reconfigurable defects are introduced by fastening threaded rods with nuts to a perforated two-dimensional phononic crystal slab. Two types of defects are defined based on the assembly length of the rod, so that the latter resonates at different frequencies. By coupling parallel waveguides, space and frequency demultiplexers operating at resonant frequencies are designed and fabricated. Manipulation of Lamb waves is accomplished through discontinuous defect chains. Finite element analysis is employed for numerical simulations, and it is found that experimental and numerical results are in agreement, with minor deviations in the resonant frequency. This work is essential for the design and application of reconfigurable phononic devices.

Fig. 1 depicts the experimental setup. The assembly length L is defined as the distance between the top of the threaded rod and the lower surface of the upper nut, relative to the positive direction of the z-axis of the reference system. Defects are labeled either as type A ($L = 6$ mm) or type B ($L = 9$ mm) according to their length L. a is the lattice constant. Each threaded rod is clamped to the slab by four nuts, symmetrically placed on each side slab. A digital torque wrench (measurement range: 0.2 to 10 N.m, measurement accuracy: 2%) is used to apply a consistent prestress to the assembly of the rods. In the experiment, we apply a prestress of 3.5 N.m to all rods to ensure proper clamping[29]. In the numerical calculations, we apply a prestrain of 0.0067 to all rods as a corresponding boundary condition.

[a)]These authors contributed equally to this work
[b)]Corresponding Author email: wangyanfeng@tju.edu.cn

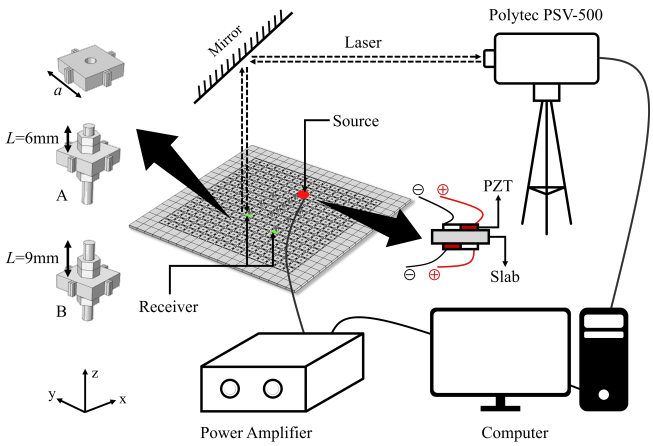

FIG. 1. Experimental setup for excitation and imaging of coupled-resonator defect chains. Two piezoelectric patches (PZTs) are attached to opposite sides of the slab and connected to a power amplifier to serve as a Lamb wave source. The source position is indicated by the red disk whereas the receiver segments positions are indicated by the green blocks. Vibrations are detected using a scanning vibrometer (Polytec PSV-500). Unit cells of the perfect PC slab and defects A ($L = 6$ mm), B ($L = 9$ mm) are shown as insets.

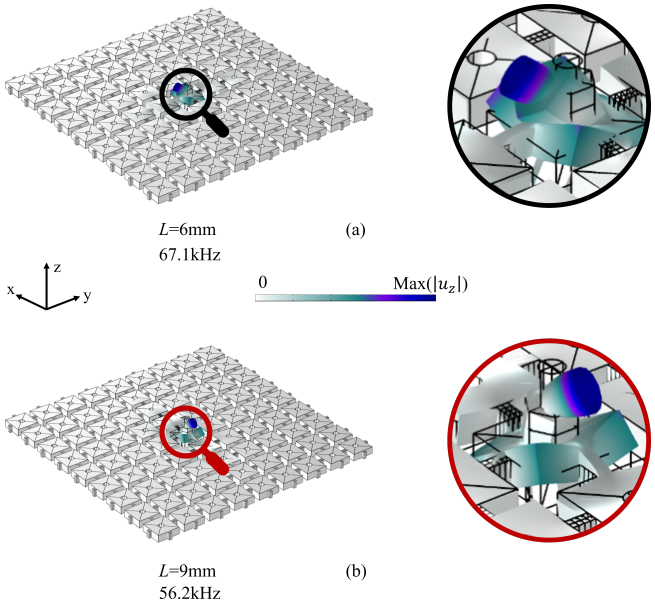

FIG. 2. Displacement fields of the defect modes for defect A ($L = 6$ mm) and defect B($L = 9$ mm). Eigenmodes at selected frequencies are displayed in panels (a) and (b). The color scale represents the normalized amplitude of the z-displacement from zero (white) to maximum (blue).

Lamb waves are excited via two piezoelectric patches (PZTs) symmetrically attached to the slab. Two vertically polarized patches are linked in opposite directions. The utilization of two patches enhances the excitation of out-of-plane vibrations. Before being applied to the PZTs, the excitation signal is amplified. Considering the limited lateral range of the excitation source, in-plane modes are inevitably excited as well[16]. A Polytec PSV-500 scanning vibrometer was used to detect and image propagating Lamb waves. Step or fixed frequency harmonic signals are utilized respectively to measure the frequency response and displacement distributions.

Numerical simulations are conducted using the 3D finite element software COMSOL. Periodic Bloch boundary conditions are applied along the x and y directions, and other interfaces are set as traction-free. Eigenmodes are obtained by selecting relevant frequencies. To distinguish different polarization modes[33], we calculate the ratio of the out-of-plane displacement to the squared total displacement via

$$p_z = \frac{\int |w|^2 \, \mathrm{d}V}{\int \left(|u|^2 + |v|^2 + |w|^2\right) \mathrm{d}V}, \tag{1}$$

where (u, v, w) represent the three components of displacement in the reference system in Fig. 1. Transmission properties are calculated by evaluating the frequency response function (FRF) as

$$T(f) = \frac{\int_{S_1} U_1 \mathrm{d}s / S_1}{\int_{S_0} U_0 \mathrm{d}s / S_0}, \tag{2}$$

where $U_0 = 1$ is the amplitude of the wave source at the excitation source (S_0) and U_1 is the total displacement collected over a receiver segment (S_1) placed at the end of the waveguide. The numerical results indicate that boundary reflections have a minimal effect on the transmission peaks. In order to reduce the noise and thus facilitate the determination of the location of the transmission peaks, low-reflective boundaries are set in the simulation. Elastic wave source and the receiver segments are set inside the slab.

First, we investigate defect modes with threaded rods and nuts. Supercells (size $9a \times 9a$) are formed to calculate the resonant frequencies of the isolated defect modes. The coupling between adjacent defects can be neglected since the size of the supercells is large enough[17]. When the threaded rod is clamped on the slab with $L = 6$ mm, the original symmetrical structure is broken, resulting in a resonant frequency at 67 kHz. Fig. 2(a) shows the eigenmodes for defect A at selected frequencies. It is observed that both the top and the bottom free end of the rod vibrates in a bending motion typical of a clamped-free beam. The mode is in fact degenerate in the x and the y directions, and can contribute to wave transmission.

When the assembly length is increased to $L = 9$ mm, the resonance frequency shifts downward to 56 kHz. The degenerate eigenmode for defect B is of the same type as for defect A, as shown in Fig. 2(b); it also contributes to wave transmission. The alteration in assembly length modifies the distribution of rods length on either side of the slab. This leads to a change in the effective length of the rods, and hence to a shift in the resonance frequency. This model explains that by manipulating the assembly length $L = 9$ mm of the defects, tunability of the resonant frequency can be achieved in the PC slab.

By coupling three parallel CREWs ($L = 6$ mm, indicated with blue wireframes), we form a spatial demultiplexer as shown in Fig. 3(a). The demultiplexer has a length of $7a$ and

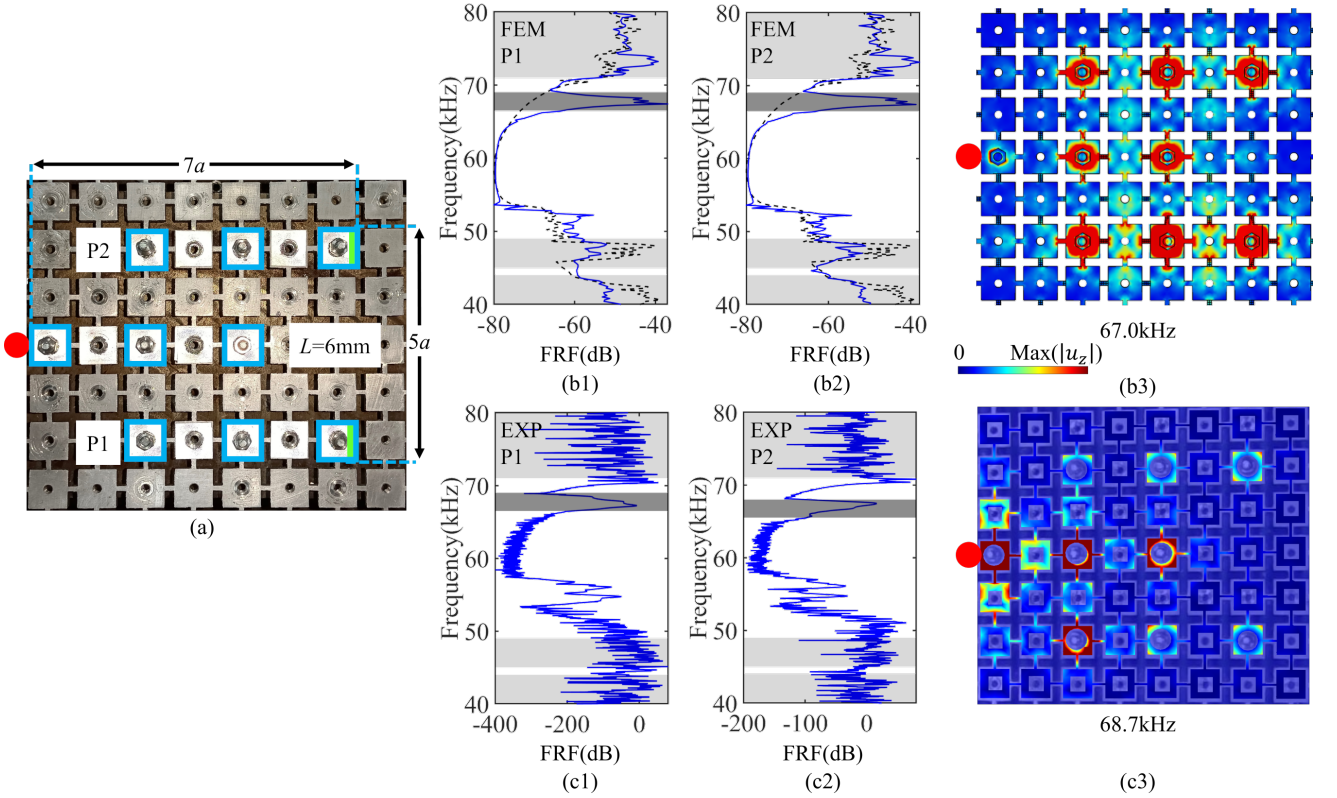

FIG. 3. Spatial demultiplexer. (a) Photograph of the sample. Numerical and experimental FRFs are shown in panels (b1), (b2) and (c1), (c2). The FRF for the perfect PC slab is plotted with a black dashed line in (b1), (b2) for comparison. The dark gray color marks the guiding bands. The light-gray color marks the passing bands for out-of-plane polarized waves in the perfect PC slab. Numerical and experimental displacement fields at selected frequencies are displayed in panels (b3) and (c3). The position of the wave source is indicated by the red disk. The positions of the receiver segments are indicated by the green blocks. The color scale represents the normalized amplitude of the z-displacement from zero (blue) to maximum (red).

a width of $5a$; each CREW has a length of $5a$. The numerical FRFs measured at the two receiver segments of the demultiplexer are presented in Fig. 3(b1) and Fig. 3(b2). We can clearly observe that the peaks are obtained around 67 kHz, corresponding to the defect mode. Figs. 3(c1) and Fig. 3(c2) present the experimental FRFs. In order to enhance the consistency of the P1 and P2 channels, we add filtering and paste reflective strips in experiments. At 55 kHz, additional transmission peaks emerge in the experimental FRFs. These deviations may be attributed to the imperfect adhesion between PZT and slab, resulting in the excitation and pickup of an in-plane mode of defect A. The other observed differences may be attributed to imperfect assembly of the rods to the slab, since the threaded structure was not considered in the simulation[17].

Numerical and experimental displacement field at the selected frequencies are shown in Fig. 3(b3) and Fig. 3(c3). The wave source is placed on the left side of the demultiplexer. Elastic waves first propagate along the central CREW. Then they couple to the upper and lower waveguides and energy is split between channels P1 and P2. The polarization of the waves are in accordance with the polarization of the defect mode. Lamb waves are tightly localized within the coupled waveguides, thereby enabling spatial demultiplexing.

As shown in Fig. 4(a), we form a frequency demultiplexer consisting of defects of type A ($L = 6$ mm, indicated with a red wireframe) and type B ($L = 9$ mm, indicated with a blue wireframe) The middle channel, N2, is made up of interleaved defects. Two CREWs (N1 and N3 channels) are placed on either side of the N2 channel, each of the three channels has a length $5a$. The frequency demultiplexer has a total length of $7a$ and a width of $5a$, as the spatial demultiplexer.

Fig. 4(b1) and Fig. 4(b2) display the numerical FRFs obtained at the two receiver segments of the demultiplexer. The FRF within the resonant frequency band is due to the defect modes. It is worth noting that the peak around 56 kHz for channel N1 does not align with the bandgap. Furthermore, an additional peak at approximately 67 kHz is evident for channel N3. These frequencies, 56 kHz and 67 kHz, represent passing bands for their respective channels. This observation implies that the coupling between channels may affect each other's response. However, this coupling effect that results in only minor response amplitudes is regarded as having a negligible impact. Different L values correspond to passing bands at different frequencies, causing the channels to resonate separately. Compared to numerical FRFs, the experimental FRFs

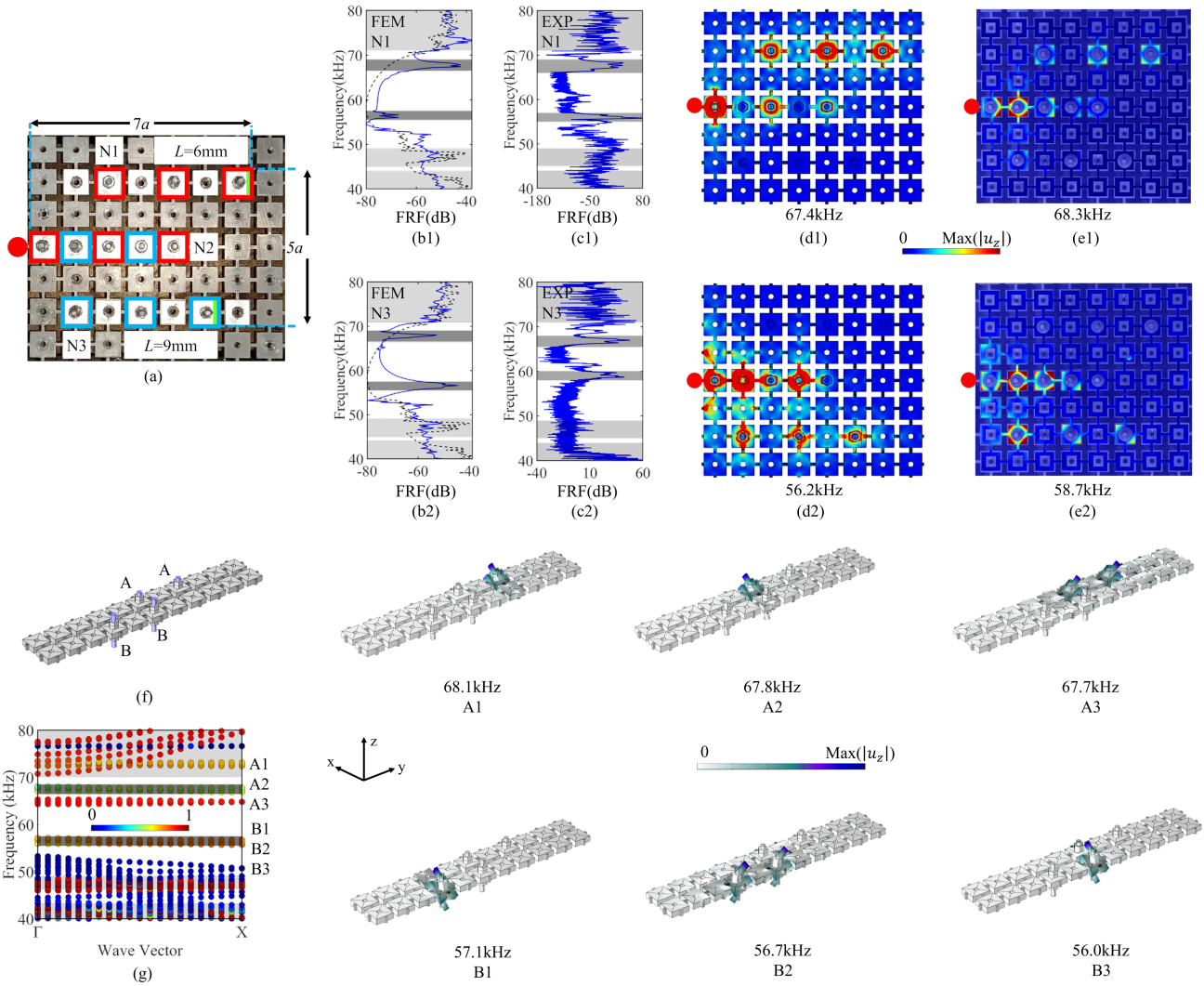

FIG. 4. Frequency demultiplexer. (a) Photograph of the sample. Numerical and experimental FRFs are shown in panels (b1), (b2) and (c1), (c2). The dark-gray color marks the guiding bands. The light-gray color marks the passing bands for out-of-plane polarized waves in the perfect PC slab. The FRF for the perfect PC slab is plotted with a black dashed line in (b1) and (b2) for comparison. Numerical and experimental displacement fields at selected frequencies are displayed in panels (d1), (d2), (e1), and (e2).The wave source position is indicated by the red disk. The receiver segments positions are indicated by the green blocks. The color scale represents the normalized amplitude of the z-displacement from zero (blue) to maximum (red). Coupled-resonator supercell (f) formed on the basis of perfect PCs with defect A and defect B. THe band structure (g) of the supercell was computed. The color bar represents the polarization from 0 (blue) to 1 (red). The light-gray areas mark the passband for the out-of-plane mode of a perfect PC slab. The dark-gray areas indicate the considered waveguiding bands. Eigenmodes at marked points A1, A2, A3 and B1, B2, B3 are listed on the right. The color scale represents the normalized amplitude of the z-displacement from zero (white) to maximum (blue).

in Fig. 4(c1) and Fig. 4(c2) show deviations in the transmission peak frequency, resonant bandwidth, and response amplitude. As with the spatial demultiplexer, the PZTs excite the in-plane mode of defect A in experiment, resulting in a larger amplitude of the transmission peak of the N1 channel at 56 kHz in Fig. 4(c1). In Fig. 4(c2), the N3 channel exhibits a significant offset at 56 kHz, which may be attributed to the symmetry of the structure of defect B[29]. This defect symmetry amplifies discrepancies between simulation and experimental results. During the construction process, some assembly defects were also identified between the rods and the slab. These may result in an uneven distribution of the force applied to the rods by the torque wrench[30].

Numerical and experimental displacement fields at the selected frequencies are shown in Fig. 4(d1), (d2) and Fig. 4(e1), (e2). The wave source is placed to the left side of the demultiplexer. Elastic waves first propagate along the hybridized channel N2. Subsequently, they couple to either the upper or the lower waveguide, continuing toward channel N1 at 67 kHz and channel N3 at 56 kHz. Nevertheless, the resonance frequencies of channels N1 and N3 experimentally deviate slightly from the numerical values. Anyway, at specific fre-

quencies, Lamb waves are successfully guided along only one of the defect chains, thereby enabling frequency demultiplexing.

To better explain the coupling between the waveguides, we formed a supercell (size $2a \times 11a$) in Fig. 4(f). In the supercell, two defects A and two defects B are arranged according to the structure at the frequency demultiplexer waveguides coupling. The band structure for the perfect waveguide is presented in Fig. 4(g), together with the defect bands for defects A and B. The presence of both red and blue bands indicates that their polarization is mixed. Two defect bands appear near 56 kHz and 67 kHz, which is consistent with the frequency of the defect modes in Fig. 2. We will not discuss the deaf band at 65kHz. According to eigenmodes at points A1, A2, A3 and B1, B2, B3 in Fig. 4, around 56kHz, defects B are resonating and defects A exhibit the vibrational form of the bandgap, whereas around 67kHz the vibrations among the two types of defects are reversed. All the eigenmodes are in fact degenerate in the x and the y directions in accordance with the defect modes shown in Fig. 2, and both can contribute to wave transmission. The supercell analysis illustrates how the frequency demultiplexer works at the waveguides coupling.

In this letter, we have presented a method for demultiplexing Lamb waves in the frequency or the space domain, based on reconfigurable coupled-resonator elastic waveguides. Through manipulation of the assembly length of threaded rods, we initially formed two different resonators with a single point defect. We then designed and fabricated wave demultiplexers. By coupling waveguides, we can modulate Lamb waves at resonant frequencies of the defects. Experimental results agree fairly well with numerical results in all cases. The present study confirms the possibility of reconfigurable wave manipulation in phononic metaplates through the coupled resonance effect. Phononic circuits operating at various frequencies can be achieved through a simple approach without the need to redesign the supporting metaplate. This type of frequency demultiplexer may have applications in signal processing. Furthermore, these findings could also be a basis for the development of advanced active and intelligent acoustic devices.

ACKNOWLEDGMENTS

The authors would like to thank Mr. Yu-Ke Ma and Mr. Tong Zhu for their help in the experiment measurement. Financial supports by the National Natural Science Foundation of China (Grant Nos. 12122207, 12021002, and 11991032), and the EIPHI Graduate School (Grant No. ANR-17-EURE-0002) are gratefully acknowledged.

DATA AVAILABILITY STATEMENT

The data that support the findings of this study are available from the corresponding author upon reasonable request.

REFERENCES

[1] Y.-F. Wang, Y.-Z. Wang, B. Wu, W. Chen, and Y.-S. Wang, "Tunable and active phononic crystals and metamaterials," Applied Mechanics Reviews **72**, 040801 (2020).
[2] S. H. Mousavi, A. B. Khanikaev, and Z. Wang, "Topologically protected elastic waves in phononic metamaterials," Nature Communications **6**, 8682 (2015).
[3] M. S. Kushwaha, P. Halevi, L. Dobrzynski, and B. Djafari-Rouhani, "Acoustic band structure of periodic elastic composites," Physical Review Letters **71**, 2022 (1993).
[4] A. Khelif and A. Adibi, "Phononic crystals," Berlin, Germany, Springer **10**, 978–1 (2015).
[5] A. Khelif, B. Aoubiza, S. Mohammadi, A. Adibi, and V. Laude, "Complete band gaps in two-dimensional phononic crystal slabs," Physical Review E **74**, 046610 (2006).
[6] M. Sigalas and E. N. Economou, "Band structure of elastic waves in two dimensional systems," Solid State Communications **86**, 141–143 (1993).
[7] V. Laude, Y. Achaoui, S. Benchabane, and A. Khelif, "Evanescent bloch waves and the complex band structure of phononic crystals," Physical Review B **80**, 092301 (2009).
[8] V. M. García-Chocano, S. Cabrera, and J. Sánchez-Dehesa, "Broadband sound absorption by lattices of microperforated cylindrical shells," Applied Physics Letters **101** (2012).
[9] M. S. Kushwaha, "Stop-bands for periodic metallic rods: Sculptures that can filter the noise," Applied Physics Letters **70**, 3218–3220 (1997).
[10] Z. Xiaopeng, L. Yan, W. Yaguang, J. Zhiyuan, and L. Yangjun, "Narrow-band filter design of phononic crystals with periodic point defects via topology optimization [j]," International Journal of Mechanical Sciences **212** (2021).
[11] V. Laude, "Principles and properties of phononic crystal waveguides," Apl Materials **9** (2021).
[12] J. O. Vasseur, O. B. Matar, J. Robillard, A.-C. Hladky-Hennion, and P. A. Deymier, "Band structures tunability of bulk 2d phononic crystals made of magneto-elastic materials," AIP Advances **1** (2011).
[13] A. Darabi, E. Kliewer, and M. J. Leamy, "Reconfigurable acoustic multiplexer/demultiplexer using time division," Applied Physics Letters **119** (2021).
[14] B. Rostami-Dogolsara, M. K. Moravvej-Farshi, and F. Nazari, "Designing switchable phononic crystal-based acoustic demultiplexer," IEEE Transactions On Ultrasonics, Ferroelectrics, Frequency Control **63**, 1468–1473 (2016).
[15] M. Miniaci, A. Marzani, N. Testoni, and L. De Marchi, "Complete band gaps in a polyvinyl chloride (pvc) phononic plate with cross-like holes: numerical design and experimental verification," Ultrasonics **56**, 251–259 (2015).
[16] Y.-F. Wang, T.-T. Wang, J.-P. Liu, Y.-S. Wang, and V. Laude, "Guiding and splitting lamb waves in coupled-resonator elastic waveguides," Composite Structures **206**, 588–593 (2018).
[17] Y.-F. Wang, T.-T. Wang, Y.-S. Wang, and V. Laude, "Reconfigurable phononic-crystal circuits formed by coupled acoustoelastic resonators," Physical Review Applied **8**, 014006 (2017).
[18] A. Yariv, Y. Xu, R. K. Lee, and A. Scherer, "Coupled-resonator optical waveguide: a proposal and analysis," Optics Letters **24**, 711–713 (1999).
[19] J. M. Escalante, A. Martínez, and V. Laude, "Dispersion relation of coupled-resonator acoustic waveguides formed by defect cavities in a phononic crystal," Journal of Physics D: Applied Physics **46**, 475301 (2013).
[20] X. An, H. Fan, and C. Zhang, "Elastic wave and vibration bandgaps in two-dimensional acoustic metamaterials with resonators and disorders," Wave Motion **80**, 69–81 (2018).
[21] R. Sainidou, N. Stefanou, and A. Modinos, "Linear chain of weakly coupled defects in a three-dimensional phononic crystal: A model acoustic waveguide," Physical Review B **74**, 172302 (2006).
[22] C. Leirer, B. Wunderlich, A. Wixforth, and M. Schneider, "Thermodynamic relaxation drives expulsion in giant unilamellar vesicles," Physical Biology **6**, 016011 (2009).

[23]T.-T. Wang, S. Bargiel, F. Lardet-Vieudrin, Y.-F. Wang, Y.-S. Wang, and V. Laude, "Collective resonances of a chain of coupled phononic microresonators," Physical Review Applied **13**, 014022 (2020).

[24]H.-w. Ji, F. Yang, A.-q. Qi, X. Wu, B. Lv, and J. Ni, "Tunable coupled-resonator acoustic waveguides based on defect resonance body," Applied Physics A **128**, 573 (2022).

[25]J. M. Escalante, A. Martínez, and V. Laude, "Dispersion relation of coupled-resonator acoustic waveguides formed by defect cavities in a phononic crystal," Journal of Physics D: Applied Physics **46**, 475301 (2013).

[26]G. Zhang and Y. Gao, "Tunability of band gaps in two-dimensional phononic crystals with magnetorheological and electrorheological composites," Acta Mechanica Solida Sinica **34**, 40–52 (2021).

[27]C. Gu and F. Jin, "Research on the tunability of point defect modes in a two-dimensional magneto-elastic phononic crystal," Journal of Physics D: Applied Physics **49**, 175103 (2016).

[28]S. Yang, X. Zhou, and Y.-F. Wang, "Tunable band gap and wave guiding in periodic grid structures with thermal sensitive materials," Composite Structures **290**, 115536 (2022).

[29]Y.-F. Wang, L. Yang, T.-T. Wang, A.-L. Chen, V. Laude, and Y.-S. Wang, "Guided lamb waves in reconfigurable phononic crystal waveguides," Apl Materials **9** (2021).

[30]W. Guo, Y.-K. Ma, Y.-F. Wang, V. Laude, and Y.-S. Wang, "Dual-tunable phononic waveguides for manipulation of guided lamb waves," Programmable Materials **1**, e11 (2023).

[31]T.-T. Wang, Y.-F. Wang, Y.-S. Wang, and V. Laude, "Tunable fluid-filled phononic metastrip," Applied Physics Letters **111** (2017).

[32]T.-T. Wang, Y.-F. Wang, Z.-C. Deng, V. Laude, and Y.-S. Wang, "Reconfigurable coupled-resonator acoustoelastic waveguides in fluid-filled phononic metaplates," Composite Structures **303**, 116355 (2023).

[33]Y. Achaoui, A. Khelif, S. Benchabane, and V. Laude, "Polarization state and level repulsion in two-dimensional phononic crystals and waveguides in the presence of material anisotropy," Journal of Physics D: Applied Physics **43**, 185401 (2010).

[34]T.-T. Wang, S. Bargiel, F. Lardet-Vieudrin, Y.-F. Wang, Y.-S. Wang, and V. Laude, "Phononic coupled-resonator waveguide micro-cavities," Applied Sciences **10**, 6751 (2020).